BIOCHIMICA ET BIOPHYSICA ACTA
BBA

Alamethicin channels – modelling via restrained molecular dynamics simulations

J. Breed [a,1], P.C. Biggin [a], I.D. Kerr [a], O.S. Smart [b], M.S.P. Sansom [a,*]

[a] *Laboratory of Molecular Biophysics, University of Oxford, The Rex Richards Building, South Parks Road, Oxford OX1 3QU, UK*
[b] *Department of Crystallography, Birkbeck College, University of London, Malet Street, London WC1 7HX, UK*

Received 17 September 1996; accepted 17 December 1996

Abstract

Alamethicin channels have been modelled as approximately parallel bundles of transbilayer helices containing between $N = 4$ and 8 helices per bundle. Initial models were generated by in vacuo restrained molecular dynamics (MD) simulations, and were refined by 60 ps MD simulations with water molecules present within and at the mouths of the central pore. The helix bundles were stabilized by networks of H-bonds between intra-pore water molecules and Gln-7 side-chains. Channel conductances were predicted on the basis of pore radius profiles, and suggested that the $N = 4$ bundle formed an occluded pore, whereas pores with $N \geq 5$ helices per bundle were open. Continuum electrostatics calculations suggested that the $N = 6$ pore is cation-selective, whereas pores with $N \geq 7$ helices per bundle were predicted to be somewhat less ion-selective.

Keywords: Alamethicin; Peptaibol; Ion channel; Electrostatics; Channel-forming peptide

1. Introduction

Channels are ion-permeable pores present in all cell membranes, from prokaryotes to mammals and higher plants. Consequently, there is considerable interest in understanding the molecular basis of channel function. This is hampered by a dearth of atomic resolution structural data for ion channel proteins. One way around this problem is to investigate channel-forming peptides (CFPs; [1]), for which both X-ray and NMR data are available. Alamethicin (Alm), a member of the peptaibol family of CFPs, is a 20 residue peptide whose conformation, interactions with lipid bilayers and channel-forming properties have been intensively investigated for over a decade [2–4]. The sequence of Alm contains a strongly helix-promoting amino acid, α-amino isobutyric acid (Aib). Alamethicin exists as two naturally occurring variants, the R_f30 form:

Ac-Aib-Pro-Aib-Ala-Aib-Ala-Gln^{7}-Aib-Val-Aib
-Gly-Leu-Aib-Pro^{14}-Val-Aib-Aib-Glu^{18}-Gln-Phl

and the R_f50 form in which Glu-18 is replaced by Gln-18. The N-terminus is blocked by an acetyl group and the C-terminus is a phenylalaninol (Phl), i.e., the terminal -CO_2H of phenylalanine is replaced by -CH_2OH. The high content of Aib ensures that Alm adopts a largely α-helical conformation; the

* Corresponding author. Fax: +44 1865 275182. E-mail: mark@biop.ox.ac.uk, url; http://www.indigo1.biop.ox.ac.uk
[1] Current address: Fakultät für Biologie, Universität Konstanz, Postfach 5560, M656, 78434 Konstanz, Germany.

PII S0005-2736(96)00262-3

presence of Pro-14 introduces a kink into the centre of the helix [5].

Channel-formation by Alm is strongly voltage-dependent. Once formed, the channels switch rapidly between multiple conductance levels. It is thought that the voltage-dependent step of channel formation corresponds to voltage-induced insertion of Alm into the bilayer coupled with a possible change in conformation of the helix [3–9]. The resultant inserted helices are believed to self-assemble to form parallel bundles of Alm molecules surrounding a central transbilayer pore [10–12]. The number of helices per bundle varies, resulting in Alm channels of different conductances. Within a 'burst' of Alm channel openings, switching between adjacent conductance levels (due to addition/loss of Alm helices to/from a helix bundle) occurs on a ca. 10 ms time-scale.

Ionic current measurements from single peptaibol channels enable direct determination of ion permeation properties. Such experiments support the helix bundle (or 'barrel-stave'; [6,13,14]) model, and provide constraints for molecular modelling studies of peptaibol channels. The helix bundle model is suggested by the pattern of successive conductance levels within a single burst of multi-level openings of an alamethicin channel. Increasing the number of helices in a bundle (N) increases the radius of the central pore and hence increases its conductance. The pattern of conductance levels seen upon detailed examination of experimental data is consistent with this model [13,15–17]. In principle, such data may be used to estimate numbers of helices present in an Alm bundle corresponding to a given conductance level.

In addition to electrophysiological studies of channels formed in planar lipid bilayers by Alm there is a considerable body of structural data. Both X-ray [5] and NMR studies [18] indicate that Alm forms an extended α-helix, which is kinked in its centre via a proline-induced break in its H-bonding pattern. NMR amide exchange data [19] demonstrate that Alm is largely α-helical when dissolved in methanol and retains this conformation when it interacts with lipid bilayers [20]. A number of NMR studies on Alm in solution suggest that it behaves as a relatively rigid helical rod [18,19]. However, in vacuo molecular dynamics (MD) simulations [21], NMR relaxation measurements on a spin-labelled Alm derivative [22] and multinuclear NMR studies combined with distance geometry and simulated annealing calculations [23] suggest that there may be some degree of dynamic flexibility about the proline-induced kink. Recent simulation studies of Alm/bilayer interactions [9] suggest that a small change in kink angle may occur upon insertion of the Alm helix into a bilayer, but that its overall shape is retained.

A number of models of Alm helix bundles have been proposed, starting with that of Fox and Richards [5] based on their X-ray structure for the Alm helix. The advent of more powerful computational procedures for channel modelling [24–26] and for MD simulations of ion channel models [27–30] provides an opportunity for a more detailed and rigorous computational study of Alm helix bundle models. In this paper we present models for Alm-R_f30 helix bundles with from 4 to 8 helices per bundle, and examine the steric and electrostatic properties of the pores thus generated. A preliminary account of some of this work has appeared in abstract form [31].

2. Materials and methods

2.1. General

Simulated annealing via restrained molecular dynamics (SA/MD) was run using XPLOR [32] version 3.1. Molecular dynamics (MD) simulations were performed using CHARMm [33] version 23f3. The parameter set employed was version 19, with only polar H atoms represented explicitly. Simulations were run on a DEC 2100 4/275. Structures were visualized using Quanta V4.0 (Biosym/Molecular Simulations), and diagrams were drawn using Molscript [34].

2.2. Generation of initial models

Initial models of Alm helix bundles were generated using SA/MD, as described in previous publications [25,35,36]. Briefly, a Cα template is the starting point for SA/MD, defining the initial positions of the Cα atoms of the Alm helices within a bundle, and thus embodying the assumptions discussed in the next section. The assumptions implicit in the Cα template concerning the numbers and orientation of the helices were discussed below. The remaining

backbone and side-chain atoms are superimposed on the Cα atoms of the corresponding residues. The Cα atoms of the helices remained fixed throughout *Stage* 1 of SA/MD. Annealing started at 1000 K, during which weights for covalent terms were gradually increased and a repulsive Van der Waals potential was slowly introduced after an initial delay. The system was cooled from 1000 K to 300K in steps of 10 K and 0.5 ps. Electrostatic terms were *not* included during *Stage* 1. *Stage* 1 was repeated five times for each C template, each resultant structure being subjected to 5 restrained MD runs (*Stage* 2), resulting in an ensemble of $5 \times 5 = 25$ final structures. Harmonic positional restraints were imposed on Cα atoms of the helices at the beginning of *Stage* 2, and were gradually relaxed as the temperature was reduced from 500 K to 300 K. The form of the restraining potential was:

$$E = h(\mathbf{r} - \mathbf{r}^{ref})^2$$

where $h = 20$ kcal mol^{-1}Å^{-2}. Distance restraints (both intra- and inter-helical – see below) were also introduced at this point. For these the form of the restraining potential was:

$$E = \min\left(20, \frac{2.5RT}{2c^2}\right)\Delta^2$$

where $\Delta = d\text{-}d^{TARGET}$. For inter-helix restraints $d^{TARGET} = 9.4$ Å, and $c = 0.5$ Å if $\Delta > 0$, but $c = 5.0$ Å if $\Delta < 0$. For intra-helix restraints (used to maintain backbone H-bonding patterns) values derived from standard α-helical H-bonding geometry were employed (see Ref. [25]). On reaching 300 K, a burst of 5 ps of constant temperature dynamics was performed, followed by 1000 steps of conjugate gradient energy minimization. During the latter burst of dynamics and energy minimization no positional restraints were imposed on the positions of Cα atoms, but distance restraints were maintained. During *Stage* 2 electrostatic interactions were gradually introduced into the potential energy function. All atoms were assigned partial charges as defined by the PARAM19 parameter set, and a distance-dependent dielectric ($\epsilon = r$) was used, with a switching function to smoothly truncate distant electrostatic interactions. The cpu time for generation of an ensemble of 25 structures was ca. 12 h.

2.3. Assumptions underlying the models

Initial Cα templates used as input to SA/MD (see previous section) embody a number of assumptions concerning the structure of channels formed by Alm. The first assumption is that the constituent monomers of a pore-forming bundle adopt an α-helical conformation similar to that observed in the X-ray [5] and solution NMR [18] structures. This is justified by a large body of spectroscopic data which suggests that Alm retains its α-helical conformation when interacting with lipid bilayers [20,37,38].

The second assumption is that the Alm molecules form a transmembrane bundle of approximately parallel (rather than anti-parallel) helices. Evidence in support of helix bundle formation comes from, e.g., in-plane neutron scattering data [12]. Several lines of evidence support a parallel orientation for the constituent helices of the bundle. The first is the pronounced asymmetry of Alm current–voltage curves [3]. This is strengthened by electrophysiological studies of Alm channel block by polycations [10], and by the demonstration that channels formed by covalently-linked parallel dimers of Alm helices resemble those of the parent Alm channels in their conductance values [36].

From single-channel measurements, it is evident that Alm can form channels with a range of different pore sizes, likely to correspond to bundles with different numbers of helices. An interpretation of single channel conductance data in terms of electrolyte-filled pores formed by Alm helices modelled as simple cylinders suggested that between $N = 4$ and $N \geq 8$ helices per bundle were required [3]. Interpretation of the concentration and voltage-dependence of the macroscopic conductance induced by Alm yields estimates of between $N = 4$ and $N = 11$ helices per bundle, depending upon the lipid employed [8]. Thus it is reasonable to model Alm channels using from $N = 4$ to $N = 8$ helices per bundle, whilst remembering that larger assemblies may also occur.

The other assumptions implicit in the Cα templates are that the hydrophilic surface of the Alm helix (defined by residue Gln-7) is directed towards the interior of the pore, and that the kinked helices are packed such that their N-terminal segments form closer contacts with one another than do their C-terminal segments. Both assumptions are reasonable

on energetic grounds. The hydrophilic face of a helix will prefer to face the aqueous lumen of a pore rather than the surrounding hydrophobic fatty acyl chains [39]. The C-termini of the helices carry a bulky and negatively charged Glu-18 residue, and so both steric and electrostatic considerations suggest that they will tend to repel one another, whereas the N-terminal helix segments do not carry a net charge and so are not expected to resist close packing.

On the basis of these assumptions, Cα templates for $N = 4$ to $N = 8$ Alm bundles were constructed by taking the Cα-coordinates of monomer C of the X-ray structure, and placing copies of these at the apices of symmetrical *N*-gons, with an N-terminal helix-to-helix separation of 10 Å. Trial runs suggested that the output of the SA/MD procedure was not over-sensitive to the initial helix-to-helix separation employed [40].

2.4. MD simulations of solvated pore models

From each ensemble of 25 structures generated by SA/MD, that structure closest to the average structure, as defined by structure-to-average-structure Cα atom RMSDs, was refined by MD simulations in the presence of water molecules within and at the mouths of the pore. Pore models were solvated and MD simulations performed using protocols based on those described previously [41,42]. Model pores were solvated in Quanta using pre-equilibrated boxes of water molecules. Water molecules were selected so that the central pore and the cap regions at either mouth of the pore were solvated, but such that no water molecules were present on the bilayer-exposed faces of the pores. The water model employed was a TIP3P three-site model [43] with partial charges $q_O = -0.834$ and $q_H = +0.417$, modified as in the CHARMm parameter set [44].

The solvated model pore was energy minimized prior to refinement by MD simulation. A four-stage energy minimization was performed: (a) 1000 cycles of adopted basis Newton Raphson (ABNR) minimization with the protein atoms fixed; (b) 1000 cycles of ABNR with the protein backbone atoms restrained; (c) 1000 cycles of ABNR with weak restraints on the protein Cα atoms only; and (d) 1000 cycles of ABNR with no positional restraints.

During the MD simulation a number of restraints were applied: (a) a cylindrical restraining potential on the waters [41] to prevent 'evaporation' from the mouths of the pore; (b) *intra*-helix restraints (between backbone NH and CO groups, [41]) to maintain the Alm molecules in an α-helical conformation; (c) *inter*-helix restraints (between the geometrical centres of the N-terminal segments of adjacent helices in a bundle) to hold together the helix bundle [25,26]; and (d) a 'bilayer' potential, whereby the helices were restrained to lie between two *xy*-planes set 33Å apart, in order to mimic embedding of a helix bundle within a membrane. Trial simulations with different combinations of such restraints indicated that whilst they prevented the pore model from drifting too far from the initial model, they did not substantially alter the behaviour of the water molecules either within or at the mouths of the pore, nor did they prevent some repacking of the helices.

MD simulations employed a 1 fs time-step. The system was heated from 0 to 300 K in 6 ps (5 K, 0.1 ps steps) and equilibrated for 9 ps at 300 K by rescaling of atomic velocities every 0.1 ps. The production stage of the simulation was for 60 ps, giving a total simulation time of 75 ps. Trajectories were analyzed using coordinate sets saved every 1 ps during the production stage of the simulations. Non-bonded interactions (both electrostatic and van der Waals) between distant atoms were truncated using a shift function [33] with a cut-off of 11.0 Å, and a fixed dielectric of $\epsilon = 1$ was used for electrostatic interactions. The cpu time for each MD simulation was between 40 and 50 h.

2.5. Analysis

Helix crossing angles (Ω) between adjacent N-terminal segments were determined as described in Ref. [45]. Inter-helix separations (D) were determined by calculating the distance between a pair of virtual atoms defined, in each helix, by the geometric centre of the Cα atoms of the N-terminal helix. Averages of Ω and D were determined across all adjacent helix pairs within an ensemble. The interaction energy between the helices of a bundle was defined as $\Delta E_{HH} = E(bundle)\text{-}E(isolated\ helices)$. The pore/water interaction energy of the models was defined as $\Delta E_{PW} = E(pore + water)\text{-}E(pore)\text{-}E(water)$.

Pore radius profiles were determined using HOLE [46], which yields the pore radius, $r(z)$, as a function of distance along the pore (z) axis. For each value of z the radius of a sphere is maximized whilst its centre (i.e., xy coordinates) is optimized so that the sphere is in Van der Waals contact with the nearest atom of the pore lining. Pore radius profiles were used to estimate an upper bound, G_{UPPER}, on the ionic conductance for a given model [35,47]. To achieve this a transbilayer pore was treated as an irregular cylinder of radius $r(z)$ (from HOLE) filled with an electrolyte of resistivity ρ. For a pore running from $z = a$ to

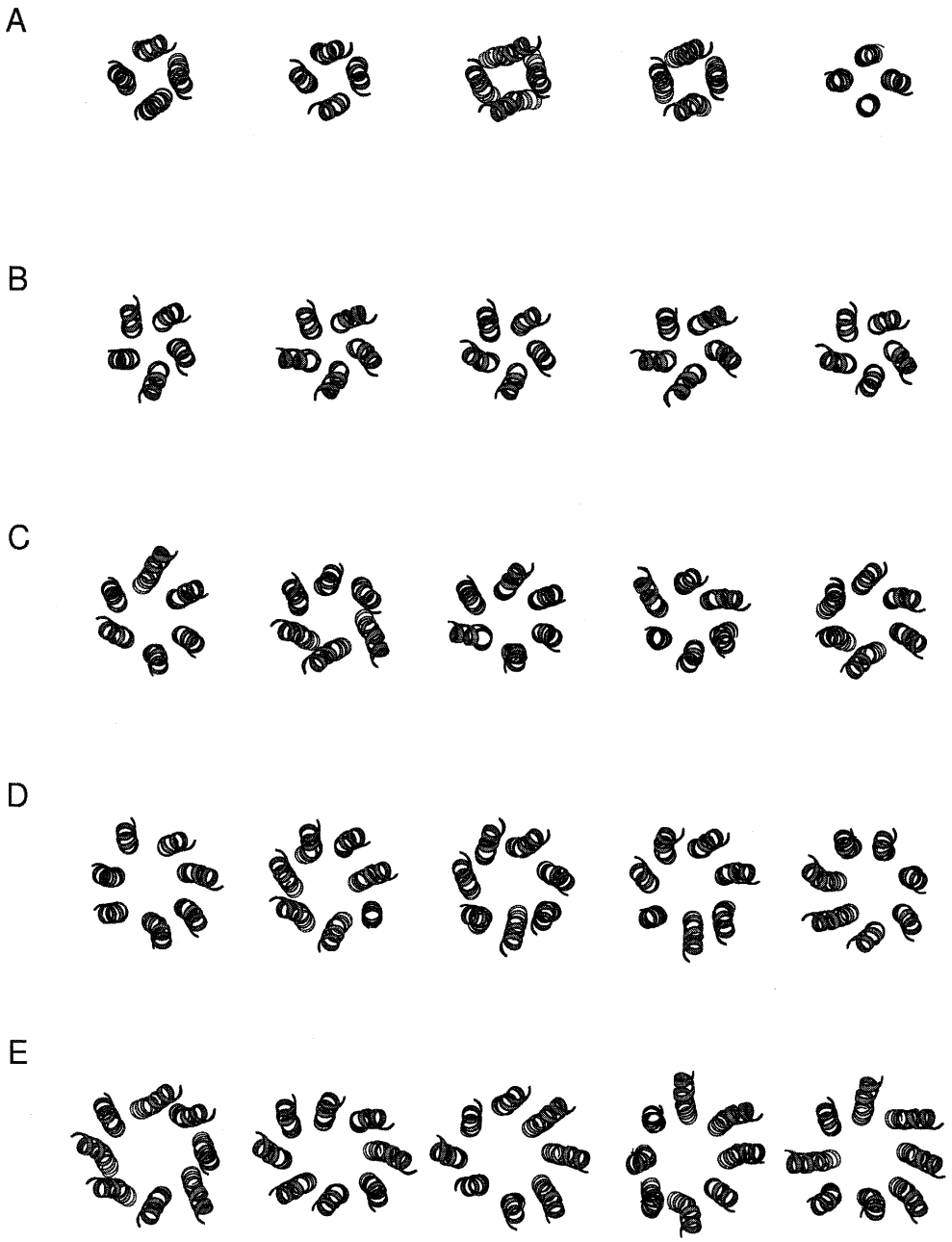

Fig. 1. Alm helix bundle models generated by SA/MD. (A) to (E) show five structures from the $N = 4$ to $N = 8$ ensembles respectively. In each case the bundle is viewed down the pore (z) axis, looking from the C-termini towards the N-termini.

$z = b$, a reasonable approximation to the electrical resistance of the pore may be obtained by integrating $\rho/(\pi r^2)$ along its length [35,48,49]. Thus, G_{UPPER} is given by the reciprocal of this resistance, i.e.:

$$G_{UPPER} = \left[\int_a^b \frac{\rho}{\pi r^2} dz\right]^{-1}.$$

Based on calculations for ion channels of known structure and conductance [47] the value of G_{UPPER} was used to predict the experimental conductance by $G_{PRED} \approx G_{UPPER}/s$, where the scale factor s varies in a linear fashion dependent upon the minimum radius of the pore, from $s = 6$ at $r_{MIN} = 1$ Å, to $s = 1$ at $r_{MIN} = 20$ Å.

Electrostatic potentials within the Alm helix bundles were calculated via numerical solution of the Poisson-Boltzmann equation, using the program UHBD [50]. The protein dielectric was set to 2 and the water dielectric to 78. Alm helix bundles were embedded in a low dielectric (2) slab of thickness 30 Å in order to mimic the effect of the surrounding protein and lipid bilayer. The ionic strength was set to 1.0 M, and 1 Å grid and a 2 Å ion exclusion (Stern) radius [51] were used. Partial atomic charges and radii used in these calculations were the same as in the MD simulations. All glutamate side-chains were assumed to be in their $-1e$ charge state. Electrostatic energy profiles were obtained by calculating the energy of a $+1e$ probe charge at successive positions along the centre of the pore, the latter being defined by HOLE calculations of pore radius profiles.

3. Results

3.1. Generating the models

Each Cα template was used to generate an ensemble of 25 structures by SA/MD in the absence of solvent molecules. Samples of five structures from each ensemble are shown in Fig. 1. It is evident that in most structures the helices form a distorted left-handed supercoil around the central pore. Although some distortion of helix backbones occurs, ensemble means of backbone ϕ and ψ angles for each residue remained close to those in the parent X-ray structure. This is consistent with results on SA/MD generation of isolated Alm helices which suggest that the X-ray structure represents a minimum potential energy conformation [9]. Variation between structures within a given ensemble suggests that a single global energy minimum for the bundle does not occur, but rather that there is a degree of flexibility in how the Alm helices may pack together. This is confirmed by backbone atom RMSDs calculated across each ensemble (Table 1).

Analysis of helix bundle geometries (Table 1) reveals that the helices pack together with their N-terminal helical segments at an inter-helical separation typical for close-packed helices (cf. an average value of 9.4 Å in a survey of helix/helix interactions [45]). For $N = 5$ to 8, helices pack together in an approximately parallel manner (i.e., Ω ca. 0°). The $N = 4$ helix bundle has a somewhat different geometry. The helices are a little further apart, and pack with a large positive crossing angle. This may reflect

Table 1
SA/MD generated models: geometry and energetics

Model	RMSD * (Å)	D § (Å)	Ω § (°)	θ_{KINK} (°)	$\Delta E_{HH}^{VDW}/N$ (kcal/mol)	$\Delta E_{HH}^{ELEC}/N$ (kcal/mol)
$N = 4$	1.7	9.8 (±0.5)	+17 (±6)	15 (±6)	−33 (±3)	−5 (±3)
$N = 5$	0.9	9.4 (±0.4)	+4 (±2)	25 (±7)	−38 (±3)	+2 (±2)
$N = 6$	2.1	9.2 (±0.4)	+3 (±6)	13 (±7)	−26 (±2)	−5 (±2)
$N = 7$	2.1	9.5 (±0.4)	+4 (±4)	18 (±6)	−28 (±2)	−2 (±2)
$N = 8$	2.4	9.5 (±0.5)	−1 (±4)	18 (±5)	−28 (±2)	0 (±2)

* Calculated for backbone atoms only. § Calculated for the N-terminal helical segments. D is the inter-helix separation and Ω the crossing angle. θ_{KINK} is the helix kink angle, ΔE_{HH}^{VDW} is the Van der Waals component of the helix/helix interaction energy, and ΔE_{HH}^{ELEC} is the electrostatic component of the helix/helix interaction energy.

the absence of a pronounced central pore from this model. For all models, the average helix kink angle lies within the range (12° to 34°) found for the 3 Alm monomers of the asymmetric unit in the X-ray structure [5]. Thus no marked distortion of the Alm helix occurs during helix bundle generation. Analysis of the helix-helix interaction energies (Table 1) does not reveal any great differences in interaction energy per helix between the different ensembles, although the $N = 5$ bundle is possibly a little more stable.

From each ensemble a representative structure was selected for refinement by a short MD simulation with TIP3P waters present within and at the mouths of the pore. The final Cα RMSD from the starting (i.e., SA/MD generated) coordinates was about 2.5 Å for each model. Cα RMSD time courses (not shown) revealed an initial rise to ca. 2.5 Å during the 15 ps heating + equilibration phase of the MD, which then remained approximately constant during the remaining 60 ps production phase indicating a reasonable degree of equilibration. Two changes in the pore structures occurred during the first 15 to 20 ps of the MD simulations. The first was a decrease in the distances between the Glu-18 side-chains of adjacent helices, from about 10 Å (Cδ to Cδ) to about 8 Å. This reflects screening of Glu-18 side-chain repulsions by intervening water molecules. The other change is a limited 'expansion' of the pores, allowing a few additional water molecules to enter. This was evident for all *N*-values. Snapshots of the $N = 4$, $N = 6$ and $N = 8$ models at the end of the MD simulation are shown in Fig. 2. It is evident that whereas in the $N = 6$ and $N = 8$ models there is a continuous water-filled pore extending all along the centre of the bundle, there is an occlusion of the pore in the $N = 4$ model. A similar occlusion, though somewhat less pronounced, is present in the $N = 5$ bundle. This suggests that the channel is 'open' only for $N \geq 6$ helices per bundle. The number of waters within the pore region ranges from ca. 60 for $N = 4$ to ca. 300 for $N = 8$.

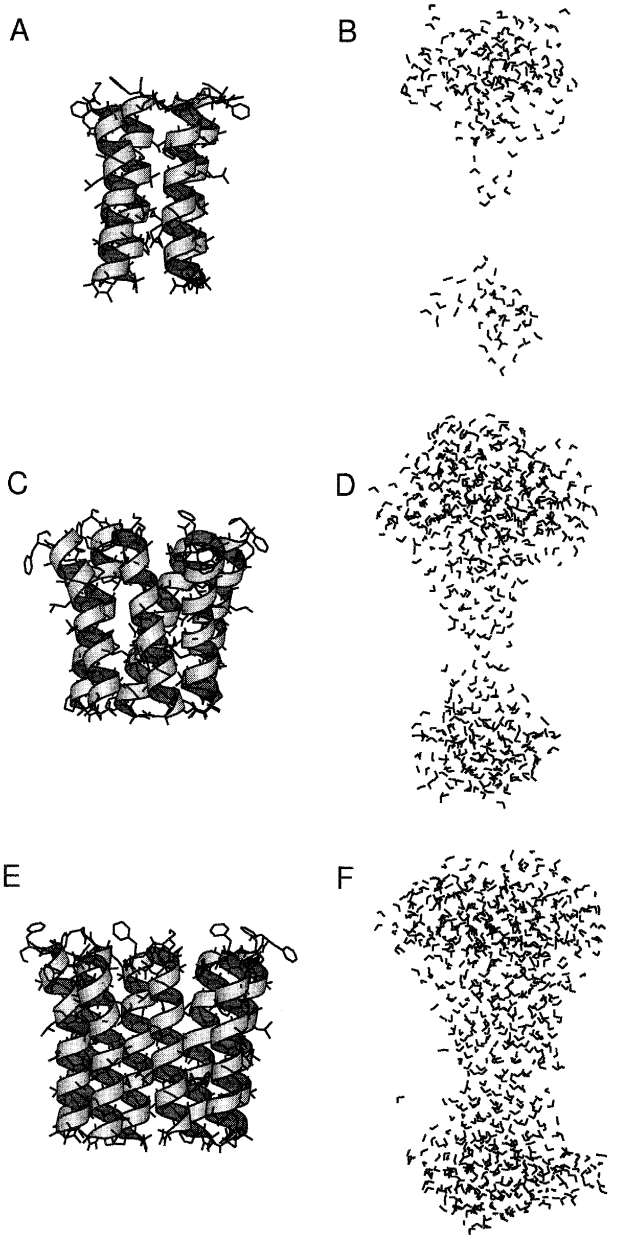

Fig. 2. Alm helix bundle models at the end of MD refinement in the presence of pore water molecules. (A), (C) and (E) show the $N = 4$, $N = 6$ and $N = 8$ models respectively; (B), (D) and (E) show the corresponding water molecules. All models are viewed perpendicular to the pore (z) axis, with the C-termini of the helices at the top of the diagram.

3.2. Structures of the bundles

The geometries of the Alm helix bundles yielded by MD refinement are summarized in Table 2. All five models exhibit limited left-handed supercoiling of the Alm helices (revealed as a positive value of Ω), this being most pronounced for the $N = 6$ bundle. The constituent helices retain kink angles similar to those of the corresponding SA/MD ensembles. Inter-helix separations are, on average, a little higher than for the SA/MD ensembles, reflecting the small

degree of expansion of the pores in the presence of water. However, overall these analyses suggest that the MD simulations in the presence of water did not result in major changes to the helix packing generated by the in vacuo simulation. The only possible change is a small decrease in the tilt of the N-terminal helix relative to the pore axis (which is presumed to be parallel to the bilayer normal), as can be seen in, e.g., Fig. 2E. This is consistent with solid state NMR data [38] which suggest that the helix axis is parallel to the bilayer normal.

The $N = 6$ pore is illustrated in Fig. 3. This reveals the two main polar side-chains which contribute to the pore lining, namely the Gln-7 and Glu-18 rings. The Glu-18 ring extends further into the channel lumen following MD refinement, as a result of solvent screening enabling closer approach of the acidic side-chains. Overall, visual inspection of the pore models reveals that the main pore-lining residues are Aib-3, Gln-7, Aib-10, Pro-14 and Glu-18. Note that in addition to the two polar residues, the carbonyl oxygen of Aib-10 is solvent exposed as a result of the disruption of H-bonding in the centre of the Alm helix by Pro-14. Thus, the channel lining may be considered as having three polar 'rings' along its length – the Gln-7 ring, the Aib-10 carbonyl ring, and the Glu-18 ring. Note that the band of aromatic Phl side-chains on the exterior surface of the bundles is located at the level of the presumed bilayer/water interface. This is consistent with the observation that aromatic residues are found in this location in membrane proteins in general [52].

3.3. Stabilization of the bundles

It is informative to examine the interactions stabilizing Alm helix bundles. In earlier molecular models

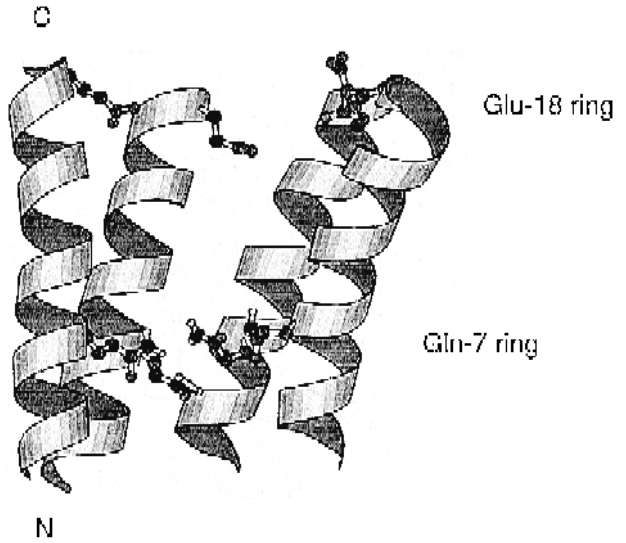

Fig. 3. The Alm $N = 6$ model. For clarity, only four helices are shown. The Gln-7 and Glu-18 sidechain are shown in ball-and-stick format.

of Alm channels [5,7] it was suggested that the Gln-7 side-chains might play a role in bundle stabilization via formation of inter-helix H-bonds, either directly or mediated by water molecules. Our simulations provide an opportunity to examine this proposal in more detail. Snapshots of the pore structures in the vicinity of Gln-7 (Fig. 4) reveal that a network of Gln-7 to water H-bonds exists. This will contribute to bundle stabilization. Detailed examination of the H-bonding patterns for different values of N reveals the situation to be rather more complex than in earlier, simpler models. For example, if one examines the total number of Gln-7 to Gln-7 plus Gln-7 to water to Gln-7 H-bonded interactions per helix interface, this declines from ca. 1 for $N = 4$ to ca. 0.25 for $N = 8$ (see Fig. 5B). However, this loss of direct and single

Table 2
MD refined models: geometry and energetics

Model	D § (Å)	Ω § (°)	θ_{KINK} (°)	$\Delta E_{HH}^{VDW}/N$ (kcal/mol)	$\Delta E_{PW}^{VDW}/N$ (kcal/mol)	$\Delta E_{PW}^{ELEC}/N$ (kcal/mol)
N = 4	9.8	+8	17	−21	−47	−255
N = 5	9.4	+5	19	−24	−60	−276
N = 6	9.6	+18	19	−25	−59	−265
N = 7	9.8	+3	18	−21	−65	−303
N = 8	9.6	+2	19	−25	−63	−303

§ Calculated for the N-terminal helical segments. ΔE_{PW}^{VDW} and ΔE_{PW}^{ELEC} are the Van der Waals and electrostatic components of the pore/water interaction energy. Other quantities are as defined in Table 1.

water bridged H-bonding interactions between Gln-7 residues as N increases is more than compensated for by a increase in the total number of Gln-7 to water H-bonds as one progresses from $N = 4$ (and $N = 5$, which is very similar) to $N \geq 6$ (Fig. 5A). This suggests that the main contribution to stabilization of the 'open' forms of the Alm channel at the level of Gln-7 is by less direct Gln-7 to water interactions. It is possible that this introduces an element of 'flexibility' into Alm channels whereby they can accommodate different numbers of helices per bundle.

In addition to solvation of the Gln-7 and Glu-18 rings there are significant numbers of H-bonds from water molecules to peptide backbone atoms. Counting H-bonds to backbone atoms as a function of residue number (data not shown) reveals that H-bonds are formed to the backbone at the two termini and in the vicinity of the proline-induced kink. The latter reinforces the suggestion that Aib-10 behaves as a hydrophilic component of the pore lining. Examination of the energetics of the helix/helix and pore/water interactions (Table 2) reveals that the electrostatic component of the pore/water interactions (H-bonds, and helix dipole/water dipole interactions) is about 10 × larger than the helix/helix interactions. This emphasizes that when attempting to

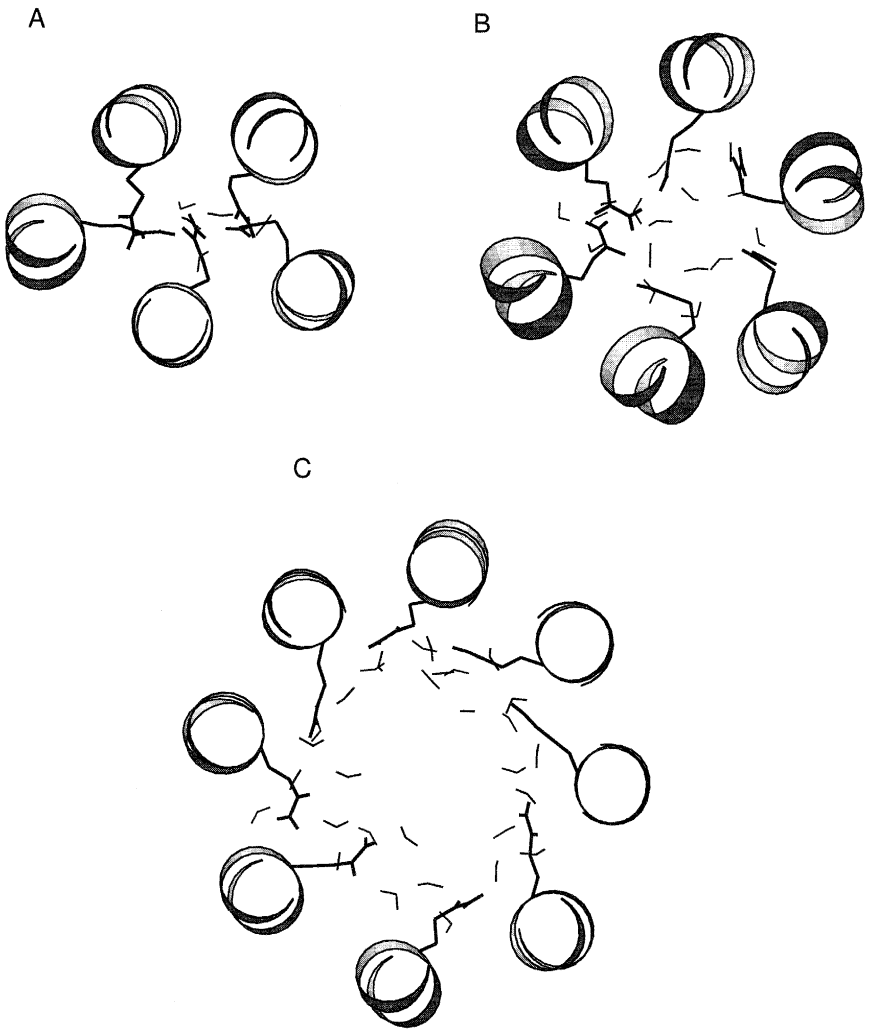

Fig. 4. The Gln-7 rings and associated water molecules of the Alm $N = 5$, $N = 6$ and $N = 8$ models. In each case the Gln-7 side-chains (thick bonds) and those water molecules forming H-bonds to them (thin bonds) are shown, viewed down the pore (z) axis.

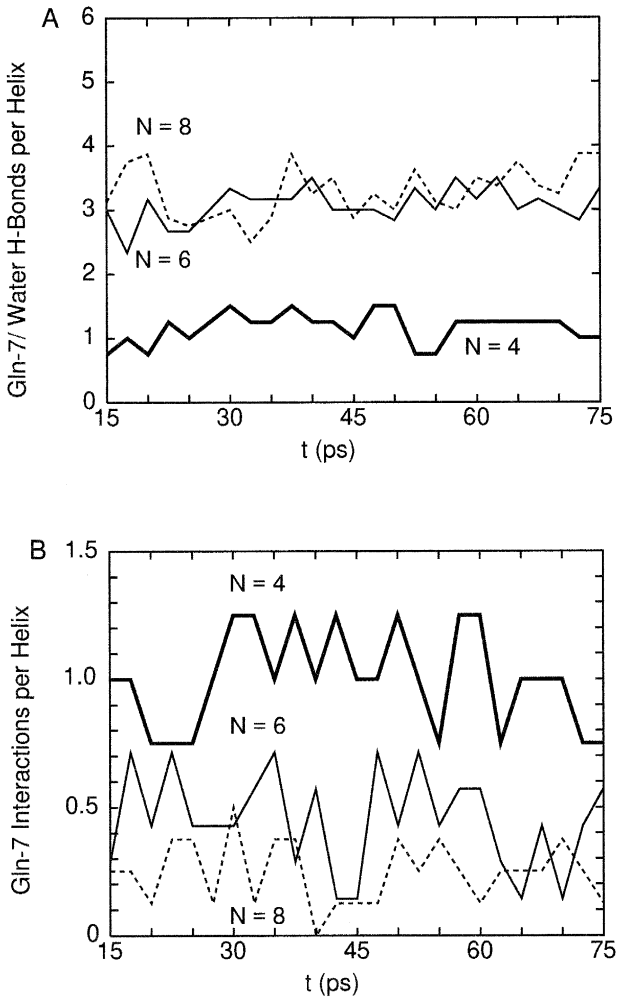

Fig. 5. H-bonding by Gln-7. (A) shows the number of H-bonds per helix between Gln-7 and a water molecule, as a function of time during the MD simulation. (B) shows the number of Gln-7 to Gln-7 interactions (both direct and indirect) per helix. In both graphs the three lines correspond to the $N = 4$ (bold), $N = 6$ (thin) and $N = 8$ (broken) models.

understand the forces stabilizing Alm helix bundles [53], it is essential to take into account intra-pore water.

3.4. Properties of the bundles

The predicted properties of the pores can be used to test the Alm bundle models against the available experimental data. Three properties have been evaluated: (i) pore radius profiles; (ii) pore conductances; and (iii) pore electrostatic profiles. Pore radius profiles were calculated using HOLE [46]. Comparison of the profiles for different values of N (Fig. 6) confirms the suggestion that the $N = 4$ pore is 'closed'. Thus, the minimum pore radius for $N = 4$ is ca. 0.5 Å, i.e., considerably less than, for example, the ionic radius of K^+ (1.3 Å). The constriction of the pore corresponds to the Gln-7 ring. A similar pore radius profile is seen for the $N = 5$ bundle. The Gln-7 side-chains also constrict the pore in the $N = 6$ and $N = 8$ models, but to a much lesser extent. Thus not only does Gln-7 appear to stabilize the bundle, but also influences the dimensions of the pore. This is in agreement with recent work on synthetic Alm analogues [53] which shows that changes to the residue at position 7 result in changes both in channel kinetics (cf. bundle stability) and in channel conductance (cf. pore radius).

Pore radius profiles allow one to predict approximate channel conductances, which may be compared with those obtained experimentally (Table 3). The first level of approximation provides an upper bound on the channel conductance (G_{UPPER}), by assuming

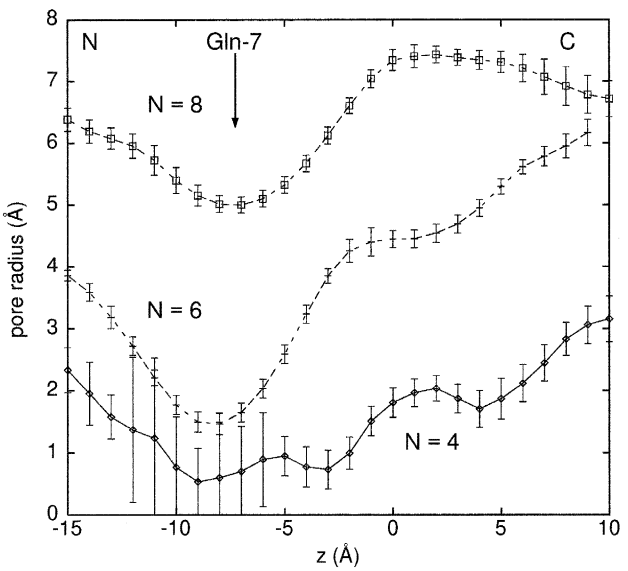

Fig. 6. Pore radius profiles, showing the pore radius as a function of distance along the pore (z) axis. The profiles for the Alm $N = 4$ (◇), $N = 6$ (+) and $N = 8$ (□) models are shown. The profiles are averages across multiple snapshots from the MD trajectories, with standard deviations shown as error bars. The N-termini of the helices are at z ca. −15 Å; the C-termini are at z ca. +10 Å, and the Gln-7 ring is at z ca. −7 Å.

that the pore is filled with an electrolyte solution with the same resistivity as the electrolyte solution in its bulk state. The values of G_{UPPER} thus obtained are all greater than the corresponding experimental conductance. By applying a scale factor obtained by comparing G_{UPPER} estimates for pores of known three dimensional structure with the corresponding experimental conductances [47], it is possible to obtain a prediction of the Alm channel conductances, G_{PRED}. The $N=4$ bundle appears to correspond to a closed channel, on the basis of the exclusion of water molecules from the middle of the pore, resulting from its low value of r_{MIN}. Thus it seems likely that the $N=5$ bundle, which has a somewhat higher value of r_{MIN} and is less occluded, may correspond to the lowest conductance level of Alm (19 pS in 1 M KCl; [17]). This conductance is somewhat over-predicted. The agreement between G_{PRED} and the observed conductance values is very good for $N=6$, and is within a factor of 2 to 3 for $N=7$ and $N=8$. This level of agreement is within the range expected and is reasonable given the considerable approximations implicit in this simple continuum model of channel conductance [47]. Thus, it seems reasonable to identify the $N=6$ bundle with the first major conductance level (ca. 300 pS in 1 M KCl) of the Alm channel.

A first approximation to the potential energy of an ion as it moves through an Alm channel may be obtained by solution of the Poisson-Boltzmann equation for the channel plus pore water embedded in a low dielectric slab. This approach has yielded qualitative agreement between model and experimental data for, e.g., the nicotinic acetylcholine receptor [54]. The results of such calculations are shown in Fig. 7, which depicts the electrostatic potential energy of a monovalent cation translated along z, following the centre of the pore as defined by HOLE. For the $N=6$ Alm pore there are two distinct energy wells, each of depth ca. -2 kcal/mol. One well is associated with the Gln-7 ring, the other with the C-terminal Glu-18 ring. The increased radius of the $N=8$ pore means that the depths of C-terminal well is reduced to ca. -1 kcal/mol, whilst the Gln-7 well has virtually disappeared. This correlates with the cation selectivity of the lower conductance levels of Alm channels, whereas higher conductance levels are considerably less selective [8,16,17].

Table 3
Pore properties

Model	r_{MIN} (Å)	G_{EXPTL} * (pS)	G_{UPPER} § (pS)	G_{PRED} † (pS)
$N=4$	0.5	–	–	–
$N=5$	0.8	19	1200	200
$N=6$	1.7	280	1700	320
$N=7$	3.7	1300	3000	600
$N=8$	5.5	2700	4300	930

r_{MIN}: minimum pore radius. * G_{EXPTL}: experimentally determined conductance in 1 M KCl, from [17]. § G_{UPPER}: upper bound on conductance, determined from pore radius profile (see Section 2). † G_{PRED}: predicted conductance, using the scaling factor of [47].

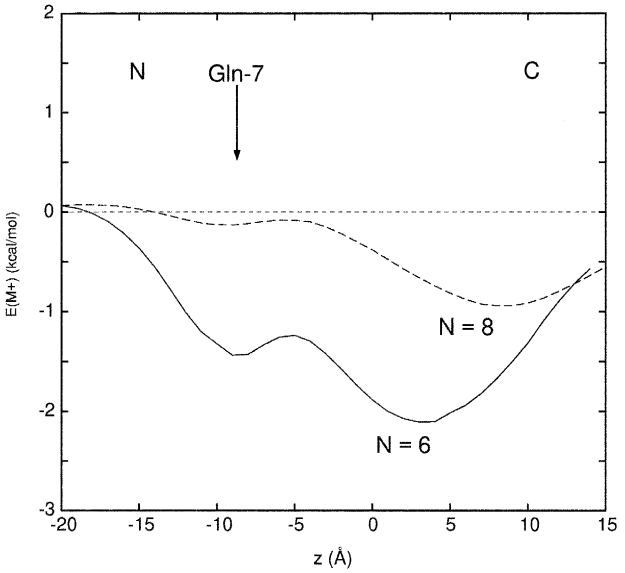

Fig. 7. Pore electrostatic potential energy profiles, for the Alm $N=6$ (solid line) and $N=8$ (broken line) models. The curves show the electrostatic potential energy, calculated via solution of the Poisson Boltzmann equation (see Section 2), of a monovalent cation moved along the centre of the pore, as defined by HOLE.

4. Discussion

4.1. Validity of the assumptions underlying the Alm pore models

Two key assumptions require examination: (i) Alm pores are formed by bundles of Alm molecules in an α-helical conformation; and (ii) the constituent helices of a bundle adopt a parallel, rather than an

anti-parallel orientation, relative to one another. A large body of spectroscopic evidence demonstrates that Alm retains its α-helical conformation both when dissolved in membrane mimetic solvents [18,19] and when in the presence of lipid bilayers [20,38]. Evidence for pore formation by bundles of Alm molecules comes from interpretation of single channel conductance level data [3] and from neutron in-plane scattering experiments [12]. In the light of this evidence, it is difficult to conclude other than that Alm channels are formed by α-helix bundles (i.e., the barrel-stave model [6,13,14]), although alternative models invoking multiple parallel pores have been discussed [55].

It has proved rather more difficult to prove that Alm channels are formed by bundles of *parallel* helices. On simple energetic grounds one might expect an anti-parallel helix bundle, in which adjacent helix dipoles are aligned anti-parallel to one another, to be more stable than a parallel bundle. Such an anti-parallel helix bundle would be symmetrical with respect to rotation about a normal to the pore (z) axis, at least for even values of N. This is inconsistent with the well documented asymmetry of the electrophysiological properties of Alm. Thus, the macroscopic current–voltage relationship of Alm is highly asymmetrical, channels only being activated at *cis*-positive potentials [8] (where the *cis* face of a membrane is that exposed to an aqueous Alm solution). Polycations will only block Alm channels when the former are present in the *cis* compartment and the voltage difference is *cis*-positive [10]. Finally, cross-linked dimers of Alm, in which two Alm helices are covalently constrained to pack parallel to one another, form ion channels whose conductance properties strongly resemble those of unmodified Alm [36]. This is again strongly indicative that a parallel helix bundle model is correct.

4.2. Critique of the modelling methodology

Initial pore models were generated by in vacuo SA/MD calculations. This method has been demonstrated to yield plausible models of pores formed by parallel α-helix bundles [25,26,42], and has also been applied to models of seven transmembrane helix bundles [56] and to pores formed by anti-parallel β-barrels [35]. The SA/MD procedure is related to a method for modelling parallel dimers of helices, which was used to successfully predict the structure of the GCN4 leucine zipper dimerization domain in advance of the subsequent X-ray and NMR structure determinations [57,58]. In the context of membrane proteins, techniques related to SA/MD have been used to model dimers of the glycophorin transmembrane helix [59], and to model the transbilayer pore formed by a pentameric bundle of phospholamban helices [60]. Thus, whilst remaining aware of the limitations of any modelling procedure, we are confident that our models merit further examination and analysis of their predicted channel properties.

A number of more technical aspects of the SA/MD procedure have been addressed. An ensemble size of 25 structures was chosen as a compromise between exhaustive sampling and low cpu times. Previous simulations on hydrophobic and Alm helix dimers [40] suggested that increasing the ensemble size to 100 would not have a marked effect on the distributions of helix bundle parameters. Cα template for the bundle models were based on monomer C from the X-ray structure of Alm. The X-ray structure was selected as being at a higher resolution than the corresponding NMR structure. However, studies of Alm helix monomers [9] indicate that the structures yielded by SA/MD are to some a large independent of the exact Cα template, provided that an α-helical template (either idealized or X-ray-derived) is used. We are therefore reasonably confident that our choice of template has not resulted in undue bias in the simulated structures.

Refinement of the initial models via MD simulations with water molecules present within and at the mouths of the pore employed procedures similar to those in previous studies of simple channel models and channel-forming peptides [26,41,42], and in studies of water within the pores of gramicidin A [28,29] and cyclic peptide nanotubes [61]. In the case of gramicidin A, for which more extensive experimental data are available, such simulations have yielded, e.g., water self-diffusion coefficients in good agreement with experimental measurements [29]. It is therefore reasonable to assume that the MD procedure yields physically meaningful results.

It is also useful to consider possible effects of the restraints imposed during the simulations. Restraints acting on water molecules consisted of a restraining

cavity of cylindrical geometry lying outside the pore formed by the protein. Thus, within the pore water molecules do not experience the restraining cavity potential. At either cap of the pore, water molecules experience a restraining potential preventing their 'evaporation' from the system. Previous simulations [62] have suggested that such a cavity potential does not substantially modify the dynamic behaviour of waters within the pore or the caps. Restraints were also applied to the Alm helices. Intra-helix distance restraints were used to maintain the α-helical geometry of Alm. Inter-helix restraints have been evaluated in a number of previous simulations [26,41]. Whilst necessary to maintain the integrity of the helix bundle, in previous simulations they did not effect the water behaviour and also did not 'force' the packing of the helices. For example, despite such restraints changes in helix crossing angle may occur [26,63].

The major omission from our simulations is that of an explicit bilayer. Inclusion of this would result in a considerable increase in cpu time, and may not be justified at this stage, i.e., for first generation models of Alm pores. As major interactions of water molecules are with one another and with the protein atoms lining the pore, omission of a lipid bilayer seems to be an acceptable first approximation. However, it is known that changes in lipid acyl tail [64] and head-group [8] can modulate Alm channel properties and so an explicit bilayer model will be required in the future.

4.3. Interpretation of results

The results of these simulation and modelling studies can be related to two main aspects of Alm channel function: (i) stability of channels formed by Alm; and (ii) open channel properties (i.e., conductance and selectivity) of the Alm pore. Since the X-ray structure determination [5], it has been suggested that H-bonds between adjacent helices could result in Gln-7 and water forming a 'hydrated Gln-7 annulus' responsible for stabilization of Alm helix bundles. This is supported by the models presented above, with the modification that interactions between adjacent helices may be bridged by more than one water molecule. Experimental support for the involvement of Gln-7 in helix bundle stabilization comes from the work of Molle et al. [53], who showed that substitution of polar side-chains smaller than glutamine at position 7 resulted in decreased channel stability, as revealed by more rapid switching between conductance levels. Molecular modelling studies on the synthetic Alm analogues employed by Molle et al. suggest that the loss of channel stability correlates with changes in H-bonding pattern between helices (Breed et al., ms. in preparation).

We have estimated pore radii for different numbers of Alm helices per bundle. Estimates of the Alm pore radius (albeit in the absence of a transbilayer voltage difference) by neutron in-plane scattering suggest a mean value of ca. 9 Å [12]. This is comparable with those estimated herein (cf. mean radius ca. 7 Å for the $N = 8$ bundle). Our values for the radii of Alm pores are somewhat lower than those estimated on the basis of polymer exclusion studies [55]. However, the interpretation of such exclusion data in terms of effective pore radii is rather complex, and it is difficult to ascertain what factors might contribute to the apparent discrepancy.

Pore radius profiles may be used to estimate approximate upper limits for channel conductances, by treating the channel as an irregular cylinder filled with electrolyte of the same resistivity as in the bulk state [35,49]. Clearly this is a major approximation, as it ignores the microscopic properties of the channel and of the solvent molecules within it, as well as failing to consider possible specific channel/ion interactions. However, we have previously shown that if one uses this approach to calculate G_{UPPER} for porins, then the resultant conductance estimates are about $5\times$ greater than the corresponding experimental values [35]. The scale factor is presumed to encapsulate the neglected microscopic properties of the channel. A more detailed study [47] suggests that the conductance may be predicted with reasonable accuracy by $G_{PRED} = G_{UPPER}/s$, where the empirical scale factor s ranges from 5 to 6 for most channels, and its exact value depends upon the minimum radius of the pore. Application of this approach to Alm gives reasonable predictions of conductances if one assumes that the first major conductance level (280 pS in 1 M KCl, Hanke 1983) corresponds to an $N = 6$ bundle. The agreement between data for the lowest conductance level (19 pS) and the prediction for the $N = 5$ bundle (200 pS) is less impressive. This is presumably because this macroscopic model

of ionic conductance breaks down for low conductance (and more ion-selective) channel states. The electrostatic properties of Alm channels can also be analyzed in an essentially macroscopic fashion, by solving the Poisson-Boltzmann equation in and around the channel. The results of such calculations are in general agreement with the observed weak cationic selectivity of Alm channels [8,17], and predict that such selectivity will decrease as N increases, again in agreement with the experiment. Overall, the level of agreement, for both conductance and selectivity, is perhaps surprising given the relative simplicity of these analytical approaches. It should be remembered that the properties of Alm channels may also be modulated by factors not included in our simulations, such as the nature of the lipid head-group and the lipid chain length. So, one should not over-emphasize the agreement between model and experiment until more inclusive simulations have been performed.

Alamethicin, for which extensive experimental data are available, demonstrates that simulation studies are valuable in allowing development of plausible models of channel structure at atomic resolution. This suggests that this approach is valid for more complex channel systems, either for channels formed by relatively simple proteins (e.g., phospholamban [65] or influenza M2 protein [66]) or for the more complex channels of excitable cell membranes, such as the nicotinic acetylcholine receptor [54]. By applying atomic resolution simulation approaches to a number of different channels, a genuinely molecular picture of the structural basis of channel function may emerge.

Acknowledgements

This research was supported by the Wellcome Trust. J.B. and P.B. thank the MRC for studentships. We also thank the Oxford Centre for Molecular Sciences for access to computer facilities.

References

[1] Sansom, M.S.P. (1991) Prog. Biophys. Mol. Biol. 55, 139–236.
[2] Woolley, G.A. and Wallace, B.A. (1992) J. Membr. Biol. 129, 109–136.
[3] Sansom, M.S.P. (1993) Q. Rev. Biophys. 26, 365–421.
[4] Cafiso, D.S. (1994) Ann. Rev. Biophys. Biomol. Struct. 23, 141–165.
[5] Fox, R.O. and Richards, F.M. (1982) Nature 300, 325–330.
[6] Baumann, G. and Mueller, P. (1974) J. Supramol. Struct. 2, 538–557.
[7] Mathew, M.K. and Balaram, P. (1983) FEBS Lett. 157, 1–5.
[8] Hall, J.E., Vodyanoy, I., Balasubramanian, T.M. and Marshall, G.R. (1984) Biophys. J. 45, 233–247.
[9] Biggin, P., Breed, J., Son, H.S. and Sansom, M.S.P. (1997) Biophys. J., in press.
[10] Rink, T., Bartel, H., Bannwarth, W. and Boheim, G. (1994) Eur. Biophys. J. 23, 155–165.
[11] Mak, D.O.D. and Webb, W.W. (1995) Biophys. J. 69, 2323–2336.
[12] He, K., Ludtke, S.J., Huang, H.W. and Worcester, D.L. (1995) Biochemistry 34, 15614–15618.
[13] Boheim, G. (1974) J. Membr. Biol. 19, 277–303.
[14] Boheim, G., Hanke, W. and Jung, G. (1983) Biophys. Struct. Mech. 9, 181–191.
[15] Gordon, L.G.M. and Haydon, D.A. (1972) Biochim. Biophys. Acta 255, 1014–1018.
[16] Gordon, L.G.M. and Haydon, D.A. (1975) Phil. Trans. Roy. Soc. Lond. B, 270, 433–447.
[17] Hanke, W. and Boheim, G. (1980) Biochim. Biophys. Acta. 596, 456–462.
[18] Esposito, G., Carver, J.A., Boyd, J. and Campbell, I.D. (1987) Biochemistry 26, 1043–1050.
[19] Dempsey, C.E. (1995) J. Am. Chem. Soc. 117, 7526–7534.
[20] Dempsey, C.E. and Handcock, L.J. (1996) Biophys. J. 70, 1777–1788.
[21] Fraternali, F. (1990) Biopolymers 30, 1083–1099.
[22] North, C.L., Franklin, J.C., Bryant, R.G. and Cafiso, D.S. (1994) Biophys. J. 67, 1861–1866.
[23] Yee, A.A., Babiuk, R. and O'Neil, J.D.J. (1995) Biopolymers 36, 781–792.
[24] Sansom, M.S.P., Balaram, P. and Karle, I. (1993) Eur. Biophys. J. 21, 369–383.
[25] Kerr, I.D., Sankararamakrishnan, R., Smart, O.S. and Sansom, M.S.P. (1994) Biophys. J. 67, 1501–1515.
[26] Kerr, I.D., Doak, D.G., Sankararamakrishnan, R., Breed, J. and Sansom, M.S.P. (1996) Prot. Eng. 9, 161–171.
[27] Åqvist, J. and Warshel, A. (1989) Biophys. J. 56, 171–182.
[28] Chiu, S.W., Jakobsson, E., Subramanian, S. and McCammon, J.A. (1991) Biophys. J. 60, 273–285.
[29] Roux, B. and Karplus, M. (1994) Ann. Rev. Biophys. Biomol. Struct. 23, 731–761.
[30] Dorman, V., Partenskii, M.B. and Jordan, P.C. (1996) Biophys. J. 70, 121–134.
[31] Breed, J. and Sansom, M.S.P. (1994) Biochem. Soc. Trans. 22, 157S.
[32] Brünger, A.T. (1992) in X-PLOR Version 3.1. A System for X-ray Crystallography and NMR, Yale University Press, New Haven, CT.
[33] Brooks, B.R., Bruccoleri, R.E., Olafson, B.D., States, D.J.,

Swaminathan, S. and Karplus, M. (1983) J. Comp. Chem. 4, 187–217.
[34] Kraulis, P.J. (1991) J. Appl. Cryst. 24, 946–950.
[35] Sansom, M.S.P. and Kerr, I.D. (1995) Biophys. J. 69, 1334–1343.
[36] You, S., Peng, S., Lien, L., Breed, J., Sansom, M.S.P. and Woolley, G.A. (1996) Biochem. 35, 6225–6232.
[37] Vogel, H. (1987) Biochem. 26, 4562–4572.
[38] North, C.L., Barranger-Mathys, M. and Cafiso, D.S. (1995) Biophys. J. 69, 2392–2397.
[39] Kerr, I.D. and Sansom, M.S.P. (1993) Eur. Biophys. J. 22, 269–277.
[40] Breed, J. (1996) D. Phil thesis, University of Oxford.
[41] Breed, J., Sankararamakrishnan, R., Kerr, I.D. and Sansom, M.S.P. (1996) Biophys. J. 70, 1643–1661.
[42] Mitton, P. and Sansom, M.S.P. (1996) Eur. Biophys. J. 25, 139–150.
[43] Jorgensen, W.L., Chandresekhar, J., Madura, J.D., Impey, R.W. and Klein, M.L. (1983) J. Chem. Phys. 79, 926–935.
[44] Venable, R.M., Brooks, B.R. and Carson, F.W. (1993) Proteins: Struct. Funct. Genet. 15, 374–384.
[45] Chothia, C., Levitt, M. and Richardson, D. (1981) J. Mol. Biol. 145, 215–250.
[46] Smart, O.S., Goodfellow, J.M. and Wallace, B.A. (1993) Biophys. J. 65, 2455–2460.
[47] Smart, O.S., Breed, J., Smith, G.R. and Sansom, M.S.P. (1997) Biophys. J., in press.
[48] Hille, B. (1992) in Ionic Channels of Excitable Membranes (2nd. edn.) Sinauer Associates, Sunderland, MA.
[49] Kuyucak, S. and Chung, S.H. (1994) Biophys. Chem. 51, 15–24.
[50] Davis, M.E., Madura, J.D., Luty, B.A. and McCammon, J.A. (1991) Comput. Phys. Comm. 62, 187–197.
[51] Gilson, M.K., Sharp, K.A. and Honig, B.H. (1988) J. Comp. Chem. 9, 327–335.
[52] Schiffer, M., Chang, C.H. and Stevens, F.J. (1992) Prot. Eng. 5, 213–214.
[53] Molle, G., Dugast, J.Y., Spach, G. and Duclohier, H. (1996) Biophys. J. 70, 1669–1675.
[54] Sankararamakrishnan, R., Adcock, C. and Sansom, M.S.P. (1996) Biophys. J. 71, 1659–1671.
[55] Bezrukov, S.M. and Vodyanoy, I. (1993) Biophys. J. 64, 16–25.
[56] Sansom, M.S.P., Son, H.S., Sankararamakrishnan, R., Kerr, I.D. and Breed, J. (1995) Biophys. J. 68, 1295–1310.
[57] Nilges, M. and Brünger, A.T. (1991) Prot. Eng. 4, 649–659.
[58] Nilges, M. and Brünger, A.T. (1993) Proteins: Struct. Func. Genet. 15, 133–146.
[59] Treutlein, H.R., Lemmon, M.A., Engelman, D.M. and Brünger, A.T. (1992) Biochemisry 31, 12726–12733.
[60] Adams, P.D., Arkin, I.T., Engelman, D.M. and Brünger, A.T. (1995) Nature Struct. Biol. 2, 154–162.
[61] Engels, M., Bashford, D. and Ghadiri, M.R. (1995) J. Amer. Chem. Soc. 117, 9151–9158.
[62] Sansom, M.S.P., Kerr, I.D., Breed, J. and Sankararamakrishnan, R. (1996) Biophys. J. 70, 693–702.
[63] Sankararamakrishnan, R. and Sansom, M.S.P. (1995) FEBS Lett. 377, 377–382.
[64] Keller, S.L., Bezrukov, S.M., Gruner, S.M., Tate, M.W., Vodyanoy, I. and Parsegian, V.A. (1993) Biophys. J. 65, 23–27.
[65] Sansom, M.S.P., Smith, G.R., Smart, O.S. and Smith, S.O. (1996) Prot. Eng., in press.
[66] Sansom, M.S.P. and Kerr, I.D. (1993) Prot. Eng. 6, 65–74.